THE ASTROPHYSICAL JOURNAL, 266:516–530, 1983 March 15

DYNAMICS OF YET MORE ELLIPTICALS AND BULGES

ROGER L. DAVIES[1,2,3,4] AND GARTH ILLINGWORTH[3,4]
Received 1982 July 16; accepted 1982 September 9

ABSTRACT

We have derived velocity dispersion profiles and rotation curves for five galaxies, four ellipticals and one probable S0 galaxy. For NGC 4839 and NGC 4889, two of the brightest galaxies in Coma, we find virtually no rotation. NGC 4839 is not an S0; it appears to be a cD galaxy, consistent with Oemler's suggestion. If so, it would be an unusual such object, being located far from the center of Coma. There are indications that the location of the very brightest ellipticals and cD galaxies is a significant factor in whether the velocity dispersion profiles in such galaxies rise or fall. NGC 584 is probably an S0. If so, it, along with NGC 128 and NGC 4594, have the most luminous bulges for which kinematical data are available. All three rotate rapidly, possibly indicating that while low luminosity bulges are similar to ellipticals of the same luminosity, bulges do not show the same decrease in rotation with luminosity as found in ellipticals. We note that bulges differ from ellipticals in other ways as well; e.g., bulges alone are found to exhibit "box"- or "peanut"-shaped structure. It appears that significant dynamical differences still exist between bulges and ellipticals. NGC 3379 appears to be consistent with being a rotationally-flattened isotropic-dispersion constant M/L oblate spheroid.

Subject headings: galaxies: internal motions — galaxies: structure

I. INTRODUCTION

Several extensive kinematical studies have shown that elliptical galaxies exhibit a wide variety of dynamical properties (Illingworth 1977; Schechter and Gunn 1979; Davies 1981; see Illingworth 1981 for a review). While ellipticals may be characterized as being dominated by anisotropy some are known to rotate quite rapidly, rapidly enough to completely account for their flattening. In addition there is evidence that the dynamical properties of elliptical galaxies depend upon their luminosity (Davies *et al.* 1983). This diversity makes it valuable to add further objects to those currently available.

We have obtained major axis spectra of NGC 584, 3379, 4839, 4889, and 6909. These have been analyzed to give rotation velocity and velocity dispersion profiles by the usual Fourier techniques for long slit data (e.g., Schechter and Gunn 1979). NGC 4839 and 4889 are two of the three brightest early-type galaxies in the Coma cluster and thus are amongst the brightest galaxies yet studied. Davies (1981) noted that NGC 3379 exhibited a gradient in velocity dispersion, sufficient to be consistent with models of constant mass-to-light ratio (M/L). Since it is common belief that most large galaxies have massive dark halos, and therefore should possess M/L profiles that increase with radius, it is important that such potential exceptions should be studied carefully. NGC 584 and 6909 both proved to illustrate the extremes of the diversity of dynamical properties exhibited by the sample of ellipticals so far studied. Basic data on these five galaxies are collected in Table 1.

[1]Institute of Astronomy, University of Cambridge.
[2]Visiting Astronomer, Kitt Peak National Observatory.
[3]Visiting Astronomer, Cerro Tololo Inter-American Observatory, which is supported by the National Science Foundation under contract AST 78-27879.
[4]Kitt Peak National Observatory, which is operated by the Association of Universities for Research in Astronomy, Inc., under contract with the National Science Foundation.

II. DATA ACQUISITION AND ANALYSIS

a) Observations

The long slit spectra analyzed here were obtained with the Ritchey-Chrétien spectrographs on the 4 m telescopes at CTIO and KPNO. Different detector systems were used on each telescope. At CTIO, photographic spectra of NGC 584 and 6909 were taken on baked IIIa-J plates with an RCA C33063 image intensifier. Spectra for the remaining galaxies were obtained using either the KPNO SIT system, the HGVS (High-Gain Video Spectrometer), or baked IIIa-J photographic plates with an RCA C33063 image intensifier. Frames taken for photometric and geometric calibration comprised sensitometer spot plates for the photographic data, bias and halogen continuum lamp frames for the HGVS, and HeNeA full slit line spectra for both detectors. The instrumental parameters are given in Table 2, while the integration times, slit position angles, and

TABLE 1

COLLECTED DATA

NGC (1)	TYPE RC2 (2)	TYPE UGC (3)	TYPE RSA (4)	ELLIPTICITY RC2[a] (5)	ELLIPTICITY Other (6)	V_0[b] (km s^{-1}) (7)	M_B^{UH}[c] (8)
584	E4	...	$S0_1(3,5)$	0.37	0.39 ± 0.04[d]	1960	−21.8
3379	E1	E	E0	0.11	0.13 ± 0.02[e]	716	−20.6
4839	S0	E	...	0.50	0.53[f]	6967	−23.2
4889	E+4	E	E4	0.31	0.30[f]	6967	−23.4
6909	E6	E	E5	0.48	0.57[f]	2610	−21.0

NOTE.—NGC 584 is also the radio source PKS 0129−07.

[a] $\varepsilon = 1 - R_{25}^{-1}$ from RC2.

[b] Group velocity from Davies *et al.* 1983 for NGC 584 and NGC 3379; V_0 from RC2 for NGC 6909; Coma mean velocity from Gregory 1975.

[c] Based on V_0 of col. (7) with $H_0 = 50$ km s^{-1} Mpc^{-1}, B_T from RC2, and $A_B = 0.133$ (cosec $|b| - 1$). For NGC 4839, $m_V = 11.62$ from Oemler 1976, and taking $\langle B - V \rangle = 1.05$ for the brightest Coma ellipticals (Sandage 1972) gives $m_B = 12.7$.

[d] Williams and Schwarzschild 1979.

[e] Wilson 1975; Barbon *et al.* 1976; de Vaucouleurs and Capaccioli 1979. ε decreases to 0.05 for $r \lesssim 10''$.

[f] $1 - b/a$ from UGC.

TABLE 2

INSTRUMENTAL PARAMETERS

PARAMETER	CTIO 4 m Photographic	KPNO 4 m HGVS	KPNO 4 m Photographic
Reciprocal dispersion (Å mm^{-1})	50	50	52
Wavelength range (Å)	3860–4540	3890–4570	4730–5615
Resolution (FWHM) (Å)	5.0	4.8	4.6[a]
Instrumental dispersion σ_i[b] (km s^{-1}) ...	150	145	120[a]
Slit length (arcmin)	3.7	2.9	3.6
Resolution along slit (arcsec) ..... (FWHM; in good seeing)	~1.5	~2.5	~1.5
Slit width (arcsec)	2.3	2.0	2.5[a]

[a] Uncertain for NGC 4889.

[b] For a Gaussian response function where σ_i = FWHM/2.35.

detector used are given in Table 3. High signal-to-noise spectra of K0 III to K2 III stars were taken for use as radial velocity and velocity dispersion templates in the usual Fourier analysis.

b) Data Reduction

This involved applying appropriate photometric and geometric rectification to the data prior to deriving velocities and velocity dispersions. Most of these steps were carried out on the Kitt Peak Interactive Picture Processing System (IPPS).

The photographic data were digitized into a 1024×330 pixel format using the PDS microdensitometer at KPNO and then transformed onto an intensity scale using the spot calibration plates. The distortion in a frame was mapped from a full slit comparison spectrum and removed, with the data being rewritten into logarithmic

TABLE 3

GALAXY OBSERVATIONS

NGC (1)	Integration (s) (2)	Position Angle[a] (degrees) (3)	Detector[b] (4)
584 ...	10400[c]	63	IT+Pg: IIIa-J (CTIO)
3379 ...	3200	65	HGVS: SIT (KPNO)
4839 ...	4800	48	HGVS: SIT (KPNO)
4839 ...	4200	65	IT+Pg: IIIa-J (KPNO)
4889 ...	3200	80	HGVS: SIT (KPNO)
4889 ...	6000	82	IT+Pg: IIIa-J (KPNO)
6909 ...	3600	67	IT+Pg: IIIa-J (CTIO)

[a] Defined E of N.

[b] Abbreviations: IT = image tube RCA C33063; Pg = Photographic plates; HGVS = High Gain Video Spectrometer utilizing a SIT vidicon.

[c] Through clouds.

wavelength intervals using a spline interpolation procedure. The "S" distortion from the image intensifier was determined from each object spectrum and removed by interpolating the data perpendicular to the dispersion.

Following this, a night sky spectrum was subtracted from the data. This spectrum was derived by averaging together many rows from the extremities of the slit. If the galaxy extended to the ends of the slit, the sky spectrum from another plate was used. The accuracy of the sky subtraction was checked by using the frame blink facility of the IPPS system.

The stellar spectra were treated in the same way as the galaxy spectra, the end product being a 1024×1 high signal-to-noise spectrum for use in the Fourier quotient analysis. The HGVS reduction differed only in that the data format was 512×128 pixels, and that bias frame subtraction and flat field division were carried out before any of the above procedures. More detailed discussion of these steps is given in Kormendy and Illingworth (1982) and Fried and Illingworth (1983).

c) *Data Analysis*

The velocity and dispersion profiles were derived using the Fourier quotient technique as described in Schechter and Gunn (1979, hereafter SG) and exhaustively tested by them and Kormendy and Illingworth (1982, hereafter KI) and Illingworth and Schechter (1982). The usual steps were taken to ensure the integrity of the method, i.e., (1) a cosine bell masking of the input spectrum, (2) removal of the mean and the low frequency components by fitting a third-order polynomial through the data, (3) interpolation across poorly subtracted night sky emission features, (4) fitting over a reasonable range in wavenumber, namely $10 < k < 300$ for the photographic spectra and $10 < k < 150$ for the HGVS data (the results were found to be relatively insensitive to the exact values chosen), and (5) comparison of the results from several template stars to demonstrate that the results were independent of the star chosen.

The fit to the quotient of the galaxy and star Fourier transforms gives a relative velocity V, a velocity dispersion σ, and a scale factor γ, and error estimates for all three. While these error estimates do seem occasionally to overestimate the true uncertainty (compare the point-to-point scatter with the error bars in the data for NGC 3379), they should at least give good relative weights for the data values.

Experiments (SG, KI) have shown that the Fourier quotient technique overestimates the velocity dispersion when it is significantly less than the instrumental resolution (for $\sigma \lesssim 0.8\ \sigma_i$, $\sigma \to \sim 0.8\ \sigma_i$). With the instrumental resolutions used here, this would indicate that dispersions of $\lesssim 120$ km s^{-1} from both the photographic data and the HGVS data should be considered upper limits.

It has also been noted (SG, KI) that the velocity dispersions derived from spectra containing the strong H and K features of Ca II (3934 Å and 3968 Å) are systematically overestimated. The velocity dispersions were derived, therefore, from a region that excluded these features, whereas the velocities were measured using the full spectrum. Scattered light in the image intensifier has affected the γ values, particularly for NGC 3379. These gradients in γ should not be interpreted as real gradients in line strength. As expected, KI found no evidence that the scattered light affected the V and σ results.

III. VELOCITY AND DISPERSION PROFILES

The V, σ, and γ results with errors are shown in Figure 1 and tabulated in Appendix A (Table 8). The data from each galaxy have been folded about the center. No significant asymmetry is apparent in any of these galaxies. The photographic data exceeded densities $D_{\rm PDS} \sim 4$ in the very centers of the galaxies. At these density levels photographic data have low signal-to-noise ratios and are susceptible to systematic calibration errors. This limited the V and σ results to radii $r \gtrsim 4''$ for NGC 584 and $r \gtrsim 2''$ for NGC 6909. Since the dispersion profile is very flat in NGC 6909, the central dispersion is unlikely to differ significantly from that at larger radii. However, this is not the case with NGC 584, where there is an obvious gradient in the dispersion. The central values found by other authors are significantly higher than our innermost dispersion measurement of 180 ± 17 km s^{-1} at $5''$. For example, Sargent *et al.* (1977) found $\sigma = 225 \pm 14$ km s^{-1}, while Tonry and Davis (1981) found 235 ± 9 km s^{-1}. We will look more closely at the dispersion profile of NGC 584 in § V*a*.

The velocity data for NGC 3379 for $r < 10''$ required beam pulling corrections. These were taken from a plot of correction factors versus SIT-target intensity established by Kormendy (1982). It seems clear from Figure 1 that the corrections applied were not large enough in this particular case. This may be because the magnitude of the distortion due to beam bending is dependent not only upon the charge level in the vicinity of the pixel being read out but also upon the form of the charge distribution on the target. Lacking a more sophisticated correction procedure, the velocities given for NGC 3379 with $r < 10''$ should only be taken as a guide to the actual shape of the rotation curve in this region. A mean curve through the points with $r < 10''$ would be an adequate approximation.

Only for NGC 3379 are rotation curves and velocity dispersion profiles available for comparison with this work (from Sargent *et al.* 1978 and Davies 1981). In general, the agreement in σ is good as we shall show in § V*c*, where we also do a detailed comparison of the NGC 3379 data with models of spherical galaxies. Direct comparison of the velocity measures is not possible

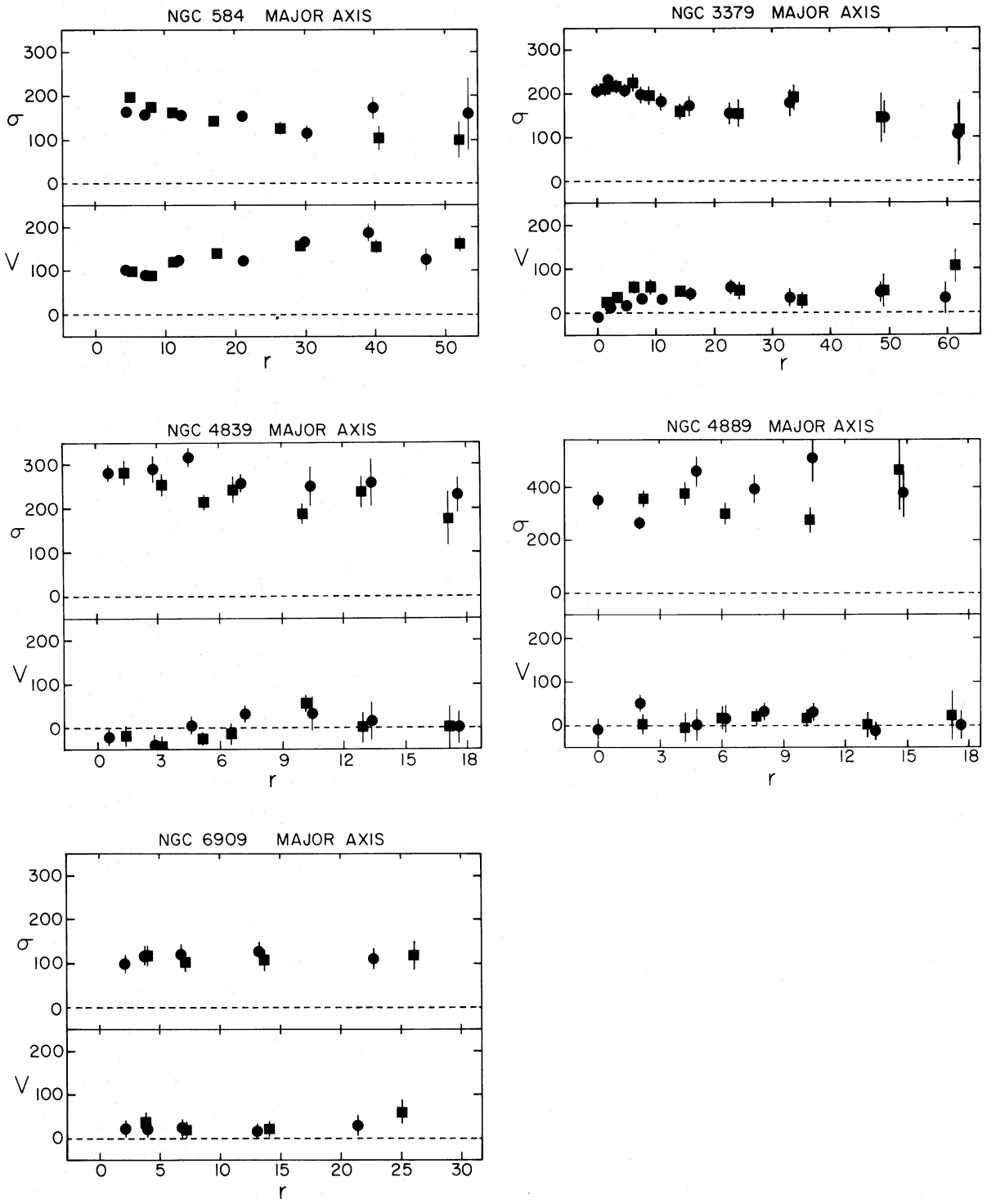

FIG. 1.—Rotation velocities V, and velocity dispersions σ, both in km s^{-1}, plotted against radius r, in arc seconds along the major axes. Note that dispersions $\sigma \sim 100$–120 km s^{-1} or less should be considered upper limits; see § II*c*. All the data are folded about the nucleus with different sides being represented by filled circles or filled squares. The position angles for the spectra are given in Table 8. Scales are 0.19 kpc arcsec^{-1} for NGC 584, 0.069 kpc arcsec^{-1} for NGC 3379, 0.68 kpc arcsec^{-1} for NGC 4839 and NGC 4889, and 0.25 kpc arcsec^{-1} for NGC 6909 (based upon $H_0 = 50$ km s^{-1} Mpc^{-1}).

as a different position angle was used by each set of authors.

The central dispersion of NGC 3379 has been measured by many authors with values ranging from 195–253 km s^{-1}. Since most of the central measurements were made with slits between 2″×4″ to 3″×12″ in size, the innermost points of the long slit data should be averaged so that the σ comparisons include light from roughly the same region of the galaxy (4″ seems appropriate). Our averaged data, weighted by the inverse square uncertainty, are compared with other sources in Table 4; there is good agreement between different sources.

The only other galaxy for which additional velocity dispersion measurements are available is NGC 4889. The aperture measurements of Faber and Jackson (1976) were made with a 2″×4″ slot, while Tonry and Davis (1981) used a 3″×12″ slot. Faber and Jackson found σ (Mg b) = 380 km s^{-1}, σ (Na D) = 400 km s^{-1}, and σ (Fourier) = 310–455 km s^{-1}, while Tonry and Davis give $\sigma = 411 \pm 20$ km s^{-1}. We find $\langle\sigma\rangle \sim 364 \pm 31$ km s^{-1} for $r < 5''$, where we have taken an unweighted mean since the point-to-point scatter is significantly larger than the error bars. This $\langle\sigma\rangle$ is somewhat lower but not inconsistent with those of Faber and Jackson and Tonry and Davis, given the uncertainty in their values and the scatter in our data. Higher signal-to-noise ratio data are needed to improve the dispersion profile in this galaxy.

TABLE 4

COMPARISON OF CENTRAL DISPERSIONS FOR NGC 3379

Source (1)	σ_0 (km s^{-1}) (2)	Aperture Size (arcsec) (3)
This paper	216±8	$r < 4$[a]
Davies 1981	219±21	$r < 4$[a]
Sargent *et al.* 1978	210±9	$r < 4$[a]
Schechter 1980	216±16	3×12
Tonry and Davis 1981	214±15	3×12
Whitmore, Kirshner, and Schechter 1979	239±23	3×10
Faber and Jackson 1976	240±23	2×4
Faber and Jackson 1976 (No Na D line)	215±24	2×4

[a]Slit data; average of all measures with $r < 4''$, weighted by the inverse square uncertainty of each.

IV. V/σ VERSUS ε

A straightforward comparison of the global dynamical properties of ellipticals with each other and with models can be made by plotting V/σ versus ε, where ε is the ellipticity. We define $V/\sigma = V_m/\bar{\sigma}$, where V_m is the maximum rotation velocity and $\bar{\sigma}$ is the mean dispersion within 0.5 r_e, r_e being the effective radius (de Vaucouleurs 1959). The justification for this is that $V_m/\sigma_0 \approx (V/\sigma)_{\text{models}}$ quite well (Binney 1980), where σ_0 is the central dispersion. While σ_0 is not well defined observationally, $\bar{\sigma}$ does, however, appear to be a good observational estimator of σ_0 (Illingworth and Schechter 1982; KI; Davies *et al.* 1982, hereafter DEFIS). Finally, $\varepsilon = 1 - (b/a)$, where b and a are the minor and major axes respectively, is the mean ellipticity within the radius range covered by the kinematical data. If such data are unavailable, then the ellipticity is derived from other sources. In these cases the radii to which ε applies is often large. DEFIS note that the RC2 values are not different *in the mean* from those derived at smaller radii. However, this is a possible source of quite significant error in ε.

The r_e, V_m, $\bar{\sigma}$, and ε values derived for the galaxies studied here, and the sources used, are given in Table 5.

TABLE 5

ROTATION-ELLIPTICITY DATA

NGC (1)	r_e (arcsec) (2)	M_B^{UH} ($H_0 = 50$) (3)	M_B^{VF} ($w = 300$) (4)	ε (5)	V_m (km s^{-1}) (6)	$\bar{\sigma}$ (km s^{-1}) (7)	$V_m/\bar{\sigma}$ (8)	$(V_m/\bar{\sigma})^*$ (9)
584	27	−21.8	−20.5	0.39±0.04	159±5	183±4	0.87±0.03	1.09±0.11
3379	59	−20.6	−19.3	0.13±0.02	45±6	200±5	0.23±0.03	0.60±0.10
4839	42:	−23.2	−22.2	0.51±0.05	23±10	255±9	0.09±0.04	0.09±0.04
4889	36	−23.4	−22.4	0.30±0.05	14±7	342±20	0.04±0.02	0.06±0.03
6909	23:	−21.0	−20.0	0.52±0.05	23±4	115±6	0.20±0.04	0.19±0.04

NOTES.—Col. (2). Effective radius $r_e = A_e/2$ from the RC2. If not available $r_e = D_{25}/6$ from the RC2. These values are marked with a colon. For NGC 584, r_e was determined from the photometry of Williams and Schwarzschild 1979. Note that r_e from $D_{25}/6$ is also 27″ for NGC 584. For NGC 3379, r_e is taken from de Vaucouleurs and Capaccioli 1979. Col. (3). Based on uniform Hubble flow distances derived from V_0 of Table 1 as noted in that Table. Col. (4). As for M_B^{UH}, except distances based on linear Virgocentric flow model with a galactic infall velocity $w = 300$ km s^{-1} from Schechter 1980 and using a distance modulus for Virgo of 30.98 from Mould, Aaronson, and Huchra 1980. Col. (5). From Table 1. Values from the RC2 and UGC are averaged and given uncertainty $\Delta\varepsilon = \pm 0.05$. Col. (6). Mean rotation velocity on the "flat" part of the rotation curve. All V weighted by ΔV^{-2} in average. Average taken for $r > 25''$ for NGC 584, $r > 12''$ for NGC 3379, $r > 6''$ for NGC 4839 and NGC 4889, $r > 5''$ for NGC 6909. Col. (7). Weighted mean of all σ for $r < r_e/2$. Weights are $(\Delta\sigma)^{-2}$. Col. (9). Observed $V_m/\bar{\sigma}$ normalized by $(V/\sigma)_{O_1}$ derived from the oblate models of Binney 1978.

The radius range used in the derivation of V_m is given in the notes to the table. The inverse square errors were used to weight each data value. Central σ values for NGC 584 from Sargent *et al.* (1977) and Tonry and Davis (1981) are averaged with our data in the derivation of $\bar{\sigma}$. Since the dispersion profile in NGC 6909 is consistent with being flat, $\bar{\sigma}$ should not be biased by the lack of dispersion measures for $r \lesssim 2''$.

The $V_M/\bar{\sigma}$ versus ϵ data of Table 5 are plotted in Fig. 2, and compared with all other available elliptical galaxy data, taken from Table 3 of DEFIS. The model lines plotted are from Binney (1978). That labeled "oblate" represents models with isotropic-residual velocity dispersions and oblate figures flattened by rotation. Such galaxies will fall on or near the oblate line regardless of inclination for $\epsilon \lesssim 0.6$ (Illingworth 1977). The line representing isotropic-dispersion prolate models differs in that it defines the *median* relation of the expected distribution in this plane on the prolate hypothesis (Binney 1978).

As is apparent here and as has often been noted, ellipticals more luminous than $M_B \sim -20.5$ are not, in general, consistent with being rotationally-flattened isotropic-dispersion oblate spheroids. However, both NGC 3379 and NGC 584 may be exceptions. Furthermore, the V/σ versus ϵ distribution for the DEFIS sample of 32 ellipticals appears to rule out these bright ellipticals, as a class, being isotropic-dispersion rotationally-flattened prolate spheroids. The median model line divides the sample not equally, but by a factor of 5 in favor of slowly rotating systems. Galaxies with $\epsilon < 0.1$ are excluded, since small ellipticities are very difficult to measure. Clearly, anisotropy plays a significant role in determining the shape of ellipticals. Whether these objects are generically oblate, prolate, or triaxial has not yet been firmly established. However, the recent results of DEFIS show that ellipticals fainter than $M_B \sim -20.5$ are consistent with being oblate spheroids, indicating that all ellipticals are likely to be oblate, or, if triaxial, close to oblate.

The present small sample does hold some surprises. First, NGC 584 is the fastest rotating elliptical yet found (in a V/σ sense). NGC 6909 is one of the slowest rotating of the very flattened objects ($\epsilon > 0.5$). The virtual absence of rotation in NGC 4839 and NGC 4889 is also noteworthy given their high luminosity and large ellipticity. We discuss these features in more detail in the following section.

V. DISCUSSION

a) NGC 584: An S0 With a Luminous, Rapidly Rotating Bulge?

NGC 584 is the most rapidly rotating bright elliptical galaxy found to date, but is it an elliptical? Could NGC 584 be an S0?

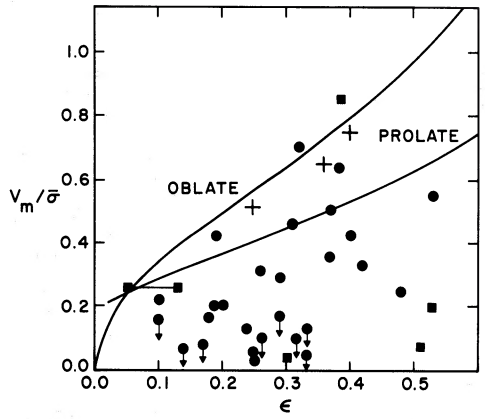

FIG. 2.—$V_m/\bar{\sigma}$ against ellipticity ϵ. The elliptical data (*filled circles*) are taken from Table 3 of Davies *et al.* 1983 for galaxies with $M_B^{UH} < -20.5$. The five ellipticals studied here (Table 5) are shown as filled squares. NGC 3379 is also shown at $\epsilon = 0.05$, its ellipticity at $r \sim 7''$ or 3 core radii (see § V*c*.). The solid line labeled "oblate" is the model relation for rotationally-flattened oblate galaxies with isotropic dispersions (Binney 1978). The "prolate" line defines the median relation for like-structured prolate galaxies. The luminous bulges ($M_B^{UH} < -21$) discussed in § V*a* (Table 6) are shown as plus signs.

In de Vaucouleurs, de Vaucouleurs, and Corwin (1976), NGC 584 is classified as an E4. In addition, the surface photometry of Williams and Schwarzschild (1979) shows it to have a high surface brightness ($\mu_V \approx$ 18.3 mag arcsec^{-2} at $r = 10''$) and to fit a power law over $15'' < r < 60''$. The surface brightness does not reach values characteristic of disks[5] until $r \gtrsim 30''$ or $r > r_e \sim 27''$ (Table 5), where $\mu_V = 20.5$ mag arcsec^{-2}. Any disk contribution to the total light must be small. Yet KI found that the presence of a disk, no matter how minimal its contribution to the total luminosity, appeared to be always associated with a rapidly rotating spheroidal component.

The evidence that NGC 584 might be an S0, while weak, is suggestive. Sandage and Tammann (1981) have classified NGC 584 from a Las Campanas 100 inch (2.5 m) plate as an $S0_1(3,5)$, distinguishing between the disk and bulge of different axial ratio. We find that the value of $V_m/\bar{\sigma}$, normalized to that for an oblate isotropic model of appropriate flattening, is $(V/\sigma)^* = 1.09 \pm 0.1$ (see Illingworth 1981; DEFIS). Thus NGC 584 is rotating rapidly, although it is not rotating significantly faster than a constant M/L, isotropic, rotationally flattened oblate galaxy. Taking the central velocity dispersion from Tonry and Davis (1981) and Sargent *et al.* (1979), and comparing the dispersion profile with a flattened, constant M/L oblate isotropic model (Binney

[5]Typical disks have $\mu_V(r = 0) \approx 20.7$ mag arcsec^{-2} and will have $\mu_V \sim 23$ mag arcsec^{-2} at $r \sim 30''$ at the distance of NGC 584 (Freeman 1970).

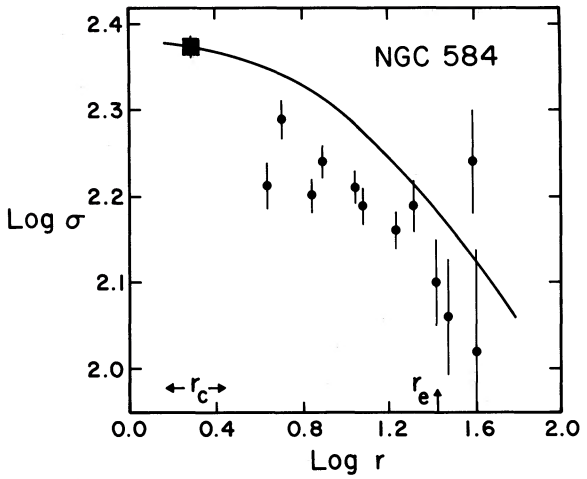

FIG. 3.—Log σ, the velocity dispersion in km s^{-1}, vs. log r, radius in arc seconds for NGC 584. The model is from Binney 1980 and is the dispersion profile expected for an E5 galaxy having a Hubble-law surface brightness profile. $r_c \sim r_e/10 \sim 3''$ was used as the radius scale for the model. The model profile was then arbitrarily fitted through the central dispersion measures. Note the steeper gradient in the data.

1980), NGC 584 is seen to show a sharper gradient than expected (Fig. 3). Finally the rotation curve rises steadily out to $r \sim r_e$, unlike the usual form for ellipticals wherein the rotation velocity is normally constant for $r > 0.1$–$0.3 r_e$.

None of these properties points unambiguously to NGC 584 being an S0. Radial anisotropy in the stellar velocity distribution could be the cause of the rapid decrease in $\sigma(r)$. The strongest hint that NGC 584 might be an S0 comes from the high rotation velocity. Why should a disk component be more apparent in the kinematic data than in the photometry? The Fourier quotient program preferentially weights narrow line components in velocity measurements from any two component average (Illingworth and Schechter 1982; see also McElroy 1981). Thus a low dispersion component (e.g., a stellar disk) enters into the velocity determination with much higher weight than just the amount of light it contributes (by factors of 3 typically for fractional light contributions of $\gtrsim 10\%$, rising in some circumstances to factors nearer ~ 10). Thus the disk component is more obvious in the velocity measurements than in the photometric data. The weight given the low dispersion component is smaller for the dispersion measurements (Whitmore 1980; McElroy 1981), and so these data are still dominated by the bulge. The result is a V/σ estimate for the bulge which is higher than the true value.

Based on the above evidence we believe that NGC 584 is likely to be an S0. The bulge-to-disk ratio, B/D, must be large, probably of the same order as that for NGC 3115, which has $B/D \sim 9$. This would make the bulge magnitude $M_B^{\rm UH} \approx -21.7$. NGC 584 is one of the brightest bulges for which dynamical data are available. DEFIS have shown that low luminosity ellipticals have high values of $(V/\sigma)^*$, similar to the bulges of the same absolute magnitude studied by KI, but that the brighter elliptical galaxies have $(V/\sigma)^*$ that is both lower in the mean and which exhibits a larger scatter. The one bright bulge in the KI sample, NGC 4594, has a high $(V/\sigma)^*$; what is $(V/\sigma)^*$ for NGC 584? At small radii, $r < 8''$, where $M_B < 19$ mag arcsec^{-2}, there can be little or no disk contamination, and yet the rotation velocity, $V_m = 94 \pm 4$ km s^{-1}. Therefore $V_m/\bar{\sigma} = 0.5$ and taking an ellipticity $\epsilon = 0.25$ for $r < 10''$ (Williams and Schwarzschild 1979), $(V/\sigma)^* = 0.9$. *The bulge of NGC 584 rotates rapidly.*

The hypothesis which suggests itself is that for bulges, $(V/\sigma)^* \approx 1$, independent of luminosity, i.e. bulges of all luminosities are oblate, isotropic rotationally-flattened spheroids. Are there other bright, high B/D objects which could be used to extend the sample? One possibility is NGC 4636 which is classified E/S0 by Sandage and Tammann (1981), and which has an $M_B^{\rm UH} \approx -21$. Kormendy (1977) suggested that this might be an S0 on photometric grounds. Using the rotation velocity (70 km s^{-1}) and dispersion ($\bar{\sigma} = 209$ km s^{-1}) from Davies (1981) and the ellipticity, $\epsilon = 0.08$, from King (1978), we find $(V/\sigma)^* = 1.1$. The problem is that NGC 4636 has very low surface brightness and the rotation velocity of the bulge, free of disk contamination, is therefore difficult to determine.

A better example is NGC 128. This "box"-shaped, edge-on S0 with $M_B^{\rm UH} = -22.3$ has been studied by Bertola and Capaccioli (1977) and Jarvis (1982). Their data shows that NGC 128 rotates on cylinders within the bulge, i.e., $V_{\rm rot}$ does not decrease with height above the plane. Thus it is straightforward to estimate V_m for the bulge, uncontaminated by disk light, i.e., $V_m = 150$ km s^{-1}. Using $\epsilon = 0.4$ and $\bar{\sigma} = 191 \pm 20$ km s^{-1} (see Table 6) we determine $V_m/\bar{\sigma} = 0.79$ and $(V_m/\sigma)^* \approx 0.95$. Taking $B/D = 1.5$, $M_B^{\rm UH}$ (bulge) $= -21.9$. Clearly NGC 128 is a rapidly rotating luminous bulge. Parameters for the three bright bulges for which data exist are given in Table 6. Although this is only a small sample, each galaxy has a high $(V/\sigma)^*$, supporting the hypothesis that bulges, unlike ellipticals, do not show a dependence of their rotational properties on luminosity.

It is interesting to consider in what ways bulges and ellipticals differ and may potentially differ:

1. Luminosity function. It is clear from the difficulty in finding bright bulges that the bright end of the luminosity function is much more fully populated in the case of elliptical galaxies than for bulges. Above a certain mass it appears that spheroids are much less likely to form disks (though it is worthwhile noting that dust-free disks will be hard to find in bright ellipticals, e.g., NGC 584!).

TABLE 6

ROTATION AND DISPERSION DATA FOR LUMINOUS BULGES

NGC (1)	M_B^{UH} (bulge) (2)	ε (3)	V_m (km s^{-1}) (4)	$\bar{\sigma}$ (km s^{-1}) (5)	$(V_m/\bar{\sigma})$ (6)	$(V_m/\bar{\sigma})^*$ (7)
128[a]	−21.9	0.40 ± 0.05	150 ± 20	191 ± 20	0.75 ± 0.09	0.91 ± 0.14[d]
584[b]	−21.7	0.25 ± 0.05	94 ± 4	183 ± 4	0.51 ± 0.02	0.88 ± 0.11[d]
4594[c]	−22.2	0.37 ± 0.08	130 ± 24	207 ± 14	0.63 ± 0.12	0.82 ± 0.21[d]

[a] M_B^{UH} (bulge) from estimated $B/D \sim 1.5$, and M_B^{UH} (total) ~ -22.3. ε and V_m are from Bertola and Capaccioli 1977, while $\bar{\sigma}$ is from Faber 1982. Bulge assumed to dominate for $r \lesssim 15''$ from photometry of Hodge and Merchant 1966.

[b] Assuming NGC 584 to be an S0; see text. V_m, σ, ε values quoted are for the bulge at $r \lesssim 10''$. ε is from Williams and Schwarzschild 1979. $B/D \sim 9$ used.

[c] Data taken from Kormendy and Illingworth 1982.

[d] Error includes uncertainty in ε.

2. Distribution of true flattenings. It is difficult to assess what the distribution of true flattenings for bulges might be. In the sample for which dynamical data are available, the bulges are much flatter on the average than the ellipticals. This is partly because the galaxies chosen for study were edge-on disk systems and are thus viewed in their equatorial plane. In the only quantitative attempt to estimate the true flattenings of spiral bulges Boroson (1981) found bulges to be on average rounder than the elliptical galaxies studied by Sandage, Freeman, and Stokes (1970). The axial ratios of the bulges were determined at a much higher surface brightness than for the ellipticals, but it is surprising that the bulges appear rounder given the greater importance of rotation to their dynamics and the flattening effect of the disk potential (Monet, Richstone and Schechter 1981). The modal value of the true flattening of elliptical galaxies is high, E3.8 (Binney and de Vaucouleurs 1981), and the mean for those KI bulges which are edge-on is E4.2. On this basis, there is no reason to postulate a substantially different distribution of true flattenings. However, Dressler and Sandage (1983) suggest that bulges are intrinsically more flattened than ellipticals of similar luminosity because, while both are oblate and supported by rotation, the bulges have higher V/σ values. This issue is sensitive to the degree of disk contamination in both the bulge rotation and axial ratio measurements of Dressler and Sandage, which is difficult to estimate. In addition, the flattenings of the small sample of low luminosity ellipticals selected for dynamical study by DEFIS may not be representative. The question of the true flattenings of bulges needs more thorough photometric investigation.

3. Rotation as a function of luminosity. It appears from the three galaxies in Table 6 that $(V/\sigma)^* \sim 1$ for bulges independent of luminosity. DEFIS showed that the average $(V/\sigma)^*$ for bright ellipticals is much lower than that for fainter galaxies ($V/\sigma \propto L^{-0.4}$), although the scatter amongst the bright galaxies is considerable.

4. A significant fraction of bulges exhibit a morphological characteristic not found in ellipticals. This is the "box" or "peanut" shape of which NGC 128 is an excellent example. Since the shape appears at small radii, it is unlikely to be due to the direct gravitational influence of the disk. In fact it appears to be causally related to the existence of differential cylindrical rotation in these objects (see KI, Davies and Illingworth 1982, and Jarvis 1982 for more detailed discussion).

These properties of bulges lead one to ask why is it that disks appear to form only in spheroids having the characteristics outlined above? That is, a high degree of rotational support, and a range of masses that does not extend to the masses of the brightest ellipticals. In addition, there is the unique relationship between "box"-shaped structure and the occurrence of a disk, and also the interesting possibility that bulges are intrinsically more flattened than ellipticals, at least for bulges and ellipticals with $M_B \gtrsim -20$.

b) *The $L \propto \sigma^n$ Relation*

Although we present results for only five galaxies, they do span the range of properties of bright ellipticals and illustrate extremes of their behavior.

In Figure 4 we present the $L \propto \sigma^n$ relation from DEFIS using their uniform Hubble flow magnitudes, M_B^{UH}, with the five galaxies observed here labeled. NGC 6909 is an extreme example of the effect reported by Terlevich *et al.* (1981) that flattened galaxies tend to have low velocity dispersions for their luminosity. At $M_B^{UH} = -21$ with $\log \sigma = 2.05$[6], NGC 6909 has a resid-

[6] The velocity dispersion for NGC 6909 is uncertain since it is close to our instrumental limit. However, we know (§ II) that the usual problem is that our dispersions tend to be *overestimated* at velocity dispersions small compared to the instrumental resolution. If so, the magnitude of the deviation for NGC 6909 may be greater than suggested here. A further measure of σ for NGC 6909 would be valuable.

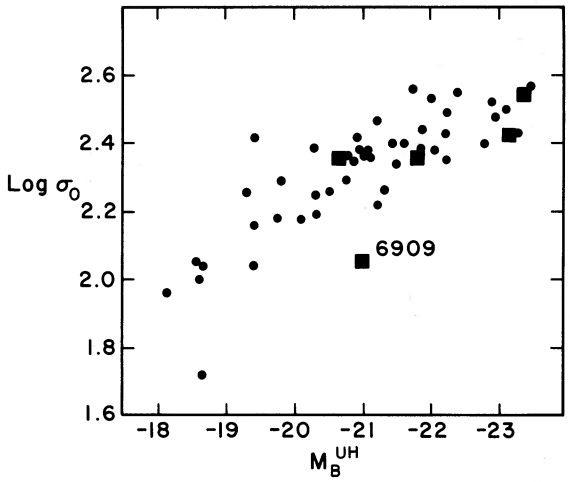

FIG. 4.—Log σ_0, the central dispersion in km s^{-1}, vs. absolute magnitude M_B^{UH} derived on the assumption of a uniform Hubble flow for the ellipticals listed in Table 3 of Davies *et al.* 1982. NGC 584, 3379, 4839, 4889, and 6909 are shown as filled squares.

ual $\Delta \log \sigma = -0.26$. With a $\log (a/b) = 0.32$ (DEFIS), NGC 6909 falls in the extreme upper left of Fig. 6*d* of Terlevich *et al.* It is a highly flattened elliptical galaxy with a large negative velocity dispersion residual. The prediction of the analysis in Terlevich *et al.* would be that NGC 6909 should also have a low Mg_2 line strength. Recently, measurements of the color of NGC 6909 indicate that it is bluer than ellipticals of similar luminosity by 0.05–0.1 magnitudes (Davies 1982). A closer investigation of the line strength and photometric properties of this galaxy might be valuable.

NGC 4839 and NGC 4887 with $M_B^{UH} < -23$ are among the brightest galaxies studied and enhance the impression that the slope of the $L \propto \sigma^n$ relation changes at $M_B \sim -21.5$. DEFIS showed that the use of Virgocentric flow magnitudes reduced this effect, but without decreasing the scatter in the relation. Whether cD galaxies will prove to fall significantly below the usual relation (e.g., Malumuth and Kirshner 1981) is still an open question. However, this could result merely from their being brightened by their well-known outer envelope. The question to be answered concerning cD's is whether the inner regions are similar to "normal" giant ellipticals. It is for the inner regions that comparisons need to be made.

c) NGC 3379: A "Normal" Galaxy?

NGC 3379 is the nearest bright elliptical. Extensive surface photometry (e.g., de Vaucouleurs and Capaccioli 1979) and kinematical data from several sources (Sargent *et al.* 1978; Davies 1981; this paper) make it an excellent "test-bed" for galaxy models. To facilitate such comparisons we have collected the velocity and velocity dispersion data from the above sources, and presented it in Table 9 (Appendix B).

One problem apparent in all three sets of data is that the internal error estimates are clearly too large; both the point-to-point scatter within each data set and between data sets are much smaller than the error bars. This is apparent in the $V(r)$ and $\sigma(r)$ profiles for NGC 3379 in Figure 1. The most likely reason is that the template star and galaxy spectra are poorly matched in all three data sets, particularly at large radii, While this mismatch is unlikely to have resulted in serious systematic biases in the velocity dispersion profiles (SG), any further observations should include a wider range of template star spectral types.

The use of formal procedures to compare models to the current data will result in very uncertain fits because of the unnecessarily large error estimates. Fortunately, enough data exist that the point-to-point scatter in the mean dispersion profile can be used to scale the error estimates. We assume that the relative error estimates are appropriate, but that the magnitude is incorrect. Accordingly we have estimated that scale factor by which the errors are overestimated and applied this factor to the data of Table 8. Different factors have been found for V and σ; the scale factors are given in Appendix B.

The V and σ data of Table 9 are plotted in Figures 5 and 6. Three different position angles, PA, were used by the various authors: 0°, 49°, and 65°. The photometric major axis is at PA $\sim 65° \pm 5°$ for $r \gtrsim 10''$ (de Vaucouleurs and Capaccioli 1979). Since $\varepsilon \lesssim 0.05$ for $r \lesssim 10''$, the major axis becomes very difficult to define

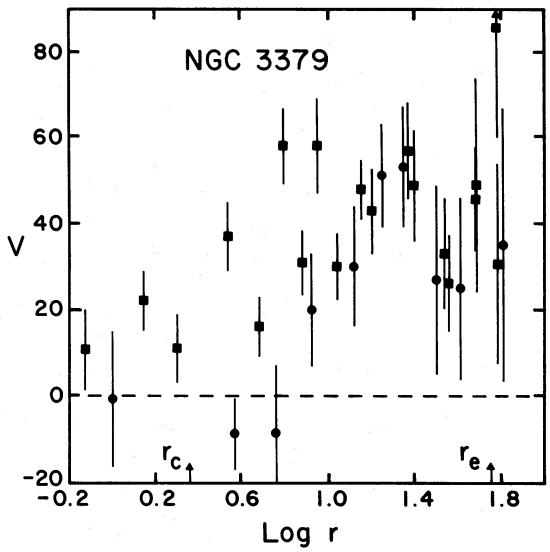

FIG. 5.—Rotation velocity V, in km s^{-1}, vs. log r, the radius in arcseconds, for NGC 3379. Filled circles are data at PA 49° from Davies 1981, while filled squares are data at PA 65° from this paper. These data are tabulated in Table 9.

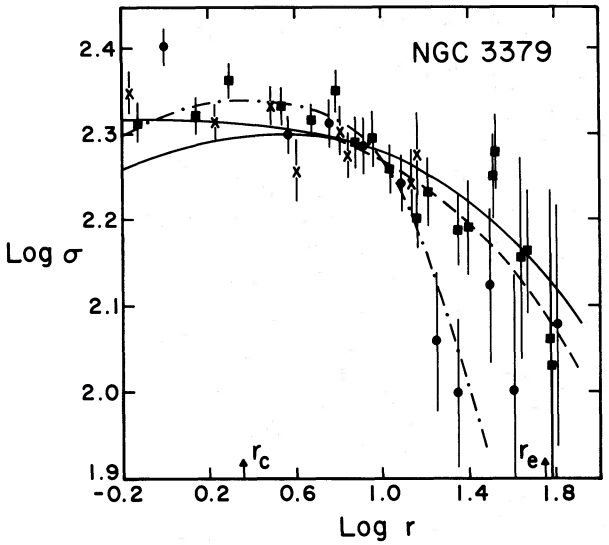

FIG. 6.—Log σ, the velocity dispersion in km s^{-1}, vs. log r, the radius in arc seconds, for NGC 3379. Data are from Table 9. Symbols are as in Fig. 5, with crosses being additional data at PA 0° from Sargent *et al.* 1978. The model dispersion profiles fitted are model D from Larson 1974 (*dash-dot line*), Binney's 1982 Boltzmann model (*solid line, high in the center*), that expected for an $r^{1/4}$-law constant-M/L galaxy from Bailey and MacDonald 1981 (*solid line, dropping in the center*), and an $r_t/r_c \sim 2.20$ constant M/L model from King 1966, 1972 (*broken line*). The Binney and King profiles are coincident in the center, as are the Binney and Bailey-MacDonald profiles at large r. The radial scaling is based on $r_c = 2''.3$ and $r_e = 59''$. The σ scaling is arbitrary and set here by eye. The model profiles have *not* been convolved with a seeing response function. As a result the difference between the model profile and the data is exaggerated at small radii, particularly for the $r^{1/4}$-law model.

at small radii. The amplitude of the rotation is very similar for both the PA 49° and PA 65° data, with $V_m \sim 50$ km s^{-1} at $8'' \lesssim r \lesssim 25''$, falling for both $r < 4''$ and for $r > 30''$. Even at PA = 0°, 65° from the major axis, some rotation is seen ($V \sim 10$ km s^{-1}; see Table 9). All three data sets show rotation in the same sense (a nontrivial result after a very complex data analysis!), with rotation velocities redshifted with respect to the systemic velocity, being SW of the minor axis at PA 155°–335°.

Rotation is dynamically significant in NGC 3379, but it is not obvious if enough is seen to fully account for its flattening. The difficulty is that the ellipticity ε increases rapidly with radius from $\varepsilon \lesssim 0.05$ for $r \lesssim 10''$ to $\varepsilon \sim 0.13$ at $r \sim 25''$ (de Vaucouleurs and Capaccioli 1979). With $V_m/\bar{\sigma} \sim 50/200 = 0.25$, $0.65 \lesssim (V_m/\bar{\sigma})^* \lesssim 1.1$ for $0.13 \gtrsim \varepsilon \gtrsim 0.05$. Binney (1980) has suggested that the ellipticity at two to three core radii, r_c, is the most appropriate for comparison of models with the kinematical data. If so, with $r_c \sim 2''.3$ (Kormendy 1977; Davies 1981) $\varepsilon \sim 0.05$ at $r \sim 3r_c \sim 7''$, and $(V_m/\bar{\sigma})^* \sim 1.1$, i.e., NGC 3379 is consistent with being a rotationally-flattened oblate spheroid with isotropic-residual velocities (see Fig. 2).

The dispersion profile in Figure 6 covers $1'' \lesssim r \lesssim 60'' \sim r_e$. The data from the three position angles agree well in the mean. Only for $r \gtrsim 30''$ is there a systematic difference, where the velocity dispersions from this paper are higher in the mean than those of Davies (1981). While this difference could be due to the poorer instrumental resolution of the current spectra, a strong case cannot be made that this is the cause of the discrepancy. We would suggest that all the data be given the same weight until further measures are made.

We have compared this dispersion profile with various models. The radial scale was set by using $r_e = 59''$ (de Vaucouleurs and Capaccioli 1979) for the Larson (1974), Bailey and MacDonald (1981), and Binney (1982) models, and choosing $r_c = 2''.3$ (Kormendy 1977; Davies 1981) for the King (1966, 1972) model. The scaling in σ is arbitrary and was made by eye. A detailed comparison (à la Binney 1980) is beyond the scope of this paper. Both the King and Binney models match the dispersion data reasonably well. A small amount of radial anisotropy may be needed to match the profiles near r_e. The dip in the center expected for an $r^{1/4}$-law model (Bailey and MacDonald 1981; Binney 1982) is not apparent in our data. In fact, the velocity dispersion may well rise more than expected from any of the models.

d) V/σ and the Brightest Ellipticals

i) *Is NGC 4839 an S0?*

NGC 4839 is classified S0 in the RC2. As kinematical data become available for a large number of objects, it will become necessary to reconcile morphological classification with the dynamical characteristics of the galaxies. If the classification S0 implies that a galaxy contains a disk population, then our data indicate that NGC 4839 is not an S0; only that it has an unusual light distribution for an elliptical.

We measure a velocity dispersion $\langle\sigma\rangle \sim 250$ km s^{-1} in NGC 4839. A disk rotating in the potential of this elliptical component will have $V_{\rm rot} \gtrsim 360$ km s^{-1}. Now $\varepsilon = 0.5$ for NGC 4839, making it unlikely that this galaxy is anything but highly inclined. If we assume that $i \gtrsim 45°$, i.e., NGC 4839 is intrinsically E6.5 or less, then the line-of-sight rotation velocity should be $V_{\rm rot} \gtrsim 250$ km s^{-1}. We find (Table 5) $V_{\rm rot} = 23 \pm 10$ km s^{-1}. The fractional contribution of a disk in NGC 4839 for $r \lesssim 18'' \sim 12 \times (50/H_0)$ kpc must be less than $33/250 = 0.13$ (where we have taken our 1 σ upper limit for $V_{\rm rot}$). In fact we know (Illingworth and Schechter 1982; see also McElroy 1981), that the Fourier quotient technique preferentially weights the low dispersion (i.e., narrow line) component in any two-component velocity average. Thus the actual contribution of disk light in NGC 4839 at any radius $\lesssim 12 \times (50/H_0)$ kpc is $\lesssim 0.10$ that of the ellipsoidal component *along the major axis*. Integrated over the whole galaxy, the disk contribution is much

smaller. NGC 4839 is clearly an elliptical dynamically, though one whose light distribution may well differ from typical elliptical galaxies.

This exemplifies the difficulty of deciding purely on morphological grounds whether an early-type galaxy is an elliptical or an S0. The clearest signature of the existence of a "cold" stellar disk is the presence of structure (e.g., stellar rings or spiral arms).

ii) *NGC 4839 as a cD*

The velocity dispersion profile has been measured in only one "classical" cD galaxy, that in the center of the cluster A2029 (Dressler 1979). The velocity dispersion was found to increase outwards. Another galaxy, IC 2082, that may well be a cD since it is the brightest and very dominant member of a rich Bautz-Morgan class I–II cluster, shows an outwardly increasing dispersion profile (Carter *et al.* 1981), though the uncertainty is large. There are indications also, that the velocity dispersion in the cD in A401 may increase outwards (Faber, Burstein, and Dressler 1977). Is this form of the dispersion profile characteristic of cD galaxies in general or is it the result of the galaxy residing in the core of the cluster?

Oemler (1976) noted that the surface brightness distribution of NGC 4839 is typical of that of cD galaxies, even though it is far from the center of the Coma cluster.[7] Given also that the luminosity of NGC 4839 is similar to that of many cD's, there appears to be no reason not to classify NGC 4839 as a cD. The shallow surface brightness gradient characteristic of cD's is a property common to S0's and could lead to confusion if such galaxies fall outside clusters.

If so, it is then of interest (Fig. 1; Table 8) that the dispersion profile in NGC 4839 appears to fall with radius. Does this indicate that the location of the very brightest galaxies is more important than their basic morphological characteristics in establishing a trend in $\sigma(r)$? Remember that a flat or increasing dispersion profile is, under very reasonable assumptions, most likely indicative of an increasing M/L in the galaxy (Illingworth 1981).[8]

[7]cD galaxies are almost invariably found in the centers of rich clusters of galaxies. However, this may be a consequence of the procedure used to define such galaxies, i.e., the contrast of such an object against its neighbor being an important part of the classification procedure. The current controversy over cD galaxies in small groups is a result of this; see, e.g., Thuan and Romanishin 1981.

[8]The assumption referred to here is that any anisotropy in the stellar velocity distribution is likely to be preferentially radial, as expected from typical collapse pictures of galaxy formation. If, however, a formation process in which the azimuthal dispersion increases preferentially with radius appears to be likely, the comments concerning M/L will need to be tempered. This could arise, for example, if merger models show such behavior and ever become an acceptable formation mechanism.

iii) *The Brightest Ellipticals*

With the previous question in mind we have gathered together data on the dynamical properties of the brightest ellipticals, those with $M_B^{UH} < -22.5$. These data are given in Table 7. The galaxies are ordered by their environment (col. [3]) with those that are isolated, in pairs, or in very small groups labeled I, those in the centers of rich clusters C, and the remainder G. M_B^{UH} is derived assuming a uniform Hubble flow with $H_0 = 50$ km s^{-1} Mpc^{-1}. The data from galaxies not in this paper are taken from Table 3 of DEFIS. $(V_m/\bar{\sigma})^*$ is the observed $V_m/\bar{\sigma}$ normalized to the oblate line of Figure 2 at the ε appropriate for each galaxy. The logarithmic gradient $d(\log\sigma)/d(\log r)$ is given in Column (10) of Table 7. Generally the dispersion profiles are consistent with being flat. However, NGC 4839 has a dispersion profile that shows a marginally significant tendency to decrease with r, while the opposite is true of A2029 and IC 2082.

While these bright ellipticals do show the very large scatter in rotation properties, characteristic of ellipticals brighter than $M_B^{UH} \sim -20$, the three galaxies NGC 4889, IC 2082, and A2029 that reside deep in clusters all show very little rotation, and flat or increasing dispersion profiles. The sample is small, however, and further data are needed to see if these dynamical properties and the implied strong M/L changes are characteristic of such central giant elliptical galaxies.

VI. CONCLUSIONS

1. Rotation and velocity dispersion profiles have been derived for four elliptical galaxies NGC 3379, NGC 4839, NGC 4889 and NGC 6909, and for the probable S0 galaxy NGC 584.

2. NGC 3379 is consistent with being a rotationally-flattened isotropic-dispersion constant M/L oblate spheroid.

3. While NGC 584 is classified E/S0, it is most likely an S0. If so, it, along with NGC 128 and NGC 4595, has the most luminous bulges for which kinematical data are available. All these rotate rapidly, indicating that while low luminosity bulges are similar to ellipticals of the same luminosity, bulges do not show the same decrease in rotation with luminosity as found by Davies *et al.* (1983) for ellipticals. Combined with the fact that bulges alone are found to exhibit "peanut"- or "box"-shaped structure, it would appear that significant dynamical differences still exist between bulges and ellipticals. In particular the possibility that bulges are intrinsically more flattened than ellipticals (at least for objects with $M_B \gtrsim -20$ where both bulges and ellipticals are rotationally flattened) has yet to be explored.

4. For NGC 4839 and NGC 4889, two of the three brightest galaxies in Coma, we find virtually no rotation. NGC 4839 is not an S0; it appears to be a cD galaxy

TABLE 7

THE BRIGHTEST ELLIPTICALS

Galaxy	Type	Environment	M_B^{UH}	ϵ	V_m	$\bar{\sigma}$r	$V_m/\bar{\sigma}$	$(V_m/\bar{\sigma})^*$	$\frac{d(\log\sigma)}{d(\log r)}$
(1)	(2)	(3)	(4)	(5)	(6)	(7)	(8)	(9)	(10)
NGC 315	E	I	−23.1	0.31	$\lesssim 30$	311 ± 11	< 0.10	< 0.15	0.028 ± 0.028
NGC 1600 ...	E	G	−22.9	0.26	$\lesssim 30$	304 ± 17	< 0.10	< 0.17	-0.046 ± 0.031
NGC 1700 ...	E	I	−22.8	0.29	74 ± 30	256 ± 10	0.29	0.45	0.063 ± 0.036
NGC 4839 ...	cD(?)	G	−23.2	0.51	23 ± 10	255 ± 9	0.09	0.09	-0.065 ± 0.027
NGC 4889 ...	E	C	−23.4	0.30	14 ± 7	342 ± 20	0.04	0.06	0.049 ± 0.041
IC 4296	E	G	−22.9	0.10	64 ± 12	291 ± 11	0.22	0.66	-0.020 ± 0.018
IC 2082	cD(?)	C	−23.3	0.33	< 31	230 ± 16	< 0.13	< 0.19	0.061 ± 0.026
A2029	cD	C	−23.4	0.33	< 20	369 ± 5	< 0.05	< 0.07	0.068 ± 0.017

NOTES.—Col. (2). Type is from RC2 or from the discussion in the text. Col. (3). Qualitative description of local environment, derived by inspection of the Palomar Sky Survey Prints or from the discussion in the relevant paper. Cols. (4)–(8). Data are from Table 5, DEFIS (Table 3), or from the original paper. V_m and $\bar{\sigma}$ are in km s^{-1}. Original sources are SG for NGC 315, 1600, 1700; Efstathiou, Ellis and Carter 1980 for IC 4296; Carter *et al.* 1981 for IC 2082; and Dressler 1979 for A2029. Col. (9). $(V_m/\bar{\sigma})$ normalized by that for oblate models $(V/\sigma)_{O\,I}$ from Binney 1978. Col. (10). Logarithmic gradient for the dispersion profiles in the above papers.

based upon Oemler's (1976) result that its surface brightness distribution is typical of cD galaxies. If so, it would be unusual amongst such objects, being located far from the center of a rich cluster (i.e., Coma).

5. Available data for the brightest ellipticals and cD galaxies suggest that environment is a significant factor in whether the dispersion profiles of such galaxies rise, stay flat, or fall.

We are grateful for the assistance given us by the staff of CTIO and KPNO. In particular, we would like to thank Paul Scott and Doug Tody for their software support, and Pat Cochrane and Betty Prewitt for their patience and care in typing the manuscript. We are grateful to Paul Schechter, James Binney, and Sandra Faber for stimulating discussions. R. L. D. is grateful to Christ's College, Cambridge for a Research Fellowship and to the Director of Kitt Peak for support during a period as a KPNO Visiting Scientist. G. I. appreciates the hospitality of the Institute of Astronomy, Cambridge, during the course of this project. The authors are particularly grateful for the support of NATO research grant RG 179.81.

APPENDIX A

The velocity V, (referenced to the systemic velocity), velocity dispersion σ, and line strength γ data are tabulated in Table 8. Errors $\Delta(V)$, $\Delta(\sigma)$, and $\Delta(\gamma)$ are also given. Radii r are in arc seconds, with negative radii for data *east* of the nucleus. V, $\Delta(V)$, σ, $\Delta(\sigma)$ are in km s^{-1}. As noted in § II the velocity data are derived from spectra containing the H and K features of Ca II, while the velocity dispersion and line strength data are from spectra that exclude these features. Occasionally, small differences may be seen in Figure 1 in the radii for corresponding V, σ, and γ points. This results from the Δ^{-2} weighting factor applied to the radii of data values that are being averaged. For tabulation purposes, we have used radii that are the mean of those for the V and σ data, except when the differences are large. In this case separate radii are given for the V data, and for the σ and γ data. Mean radii are only used where the radii differences are $\lesssim 5\%$.

The data of Table 8 are folded about the nucleus and plotted in Figure 1. The sign is changed for all velocity data *west* of the nucleus in NGC 584, and NGC 4839, and for data *east* of the nucleus in NGC 3379, NGC 4889, and NGC 6909.

The HGVS spectrum of NGC 4839 at PA 48°.2 also crossed a small galaxy 26″ SW of NGC 4839. This galaxy is redshifted by 890 ± 30 km s^{-1} from NGC 4839. It shows stellar rotation, in PA 48°, with $V_{tot} \sim 65$ km s^{-1} at a radius of $\sim 4''$, or $\sim 3\ (50/H_0)$ kpc, if at the distance of Coma. The sense of the rotation is that the SW side is redshifted. The spectrograph slit passed close to the nucleus of this galaxy; the offset and its uncertainty could be derived from good plate material, assuming that NGC 4839 was centered and that the uncertainty in the position angle is < 0°.3.

TABLE 8

ROTATIONS, DISPERSIONS, AND LINE STRENGTHS

r	V	Δ(V)	σ	Δ(σ)	γ	Δ(γ)	r	V	Δ(V)	σ	Δ(σ)	γ	Δ(γ)
		NGC 584	PA=63°										
52.0...	-162	18	100	40	0.52	0.06	10.4...	-30	37	250	44	0.50	0.08
40.3...	-155	16	105	28	0.54	0.05	7.1...	-32	18	257	19	0.70	0.05
29.3...	-156	7	...	...	...	...	4.6...	-5	19	316	20	1.05	0.08
26.4...	...	...	127	14	0.55	0.03	2.8...	40	23	290	29	1.46[b]	0.15
17.1...	-140	6	143	8	0.62	0.02	0.6...	21	15	281	18	1.50[b]	0.10
11.1...	-122	7	162	8	0.70	0.02	-1.4...	-19	23	282	27	1.44[b]	0.14
8.0...	-89	8	174	9	0.71	0.03	-3.2...	-48	21	254	24	1.09	0.10
5.1...	-99	7	196	7	0.78	0.02	-5.2...	-26	15	213	18	0.91	0.07
(0.0)[c,d]	...	...	232	8	...	...	-6.6...	-16	24	242	30	0.61	0.07
-4.4...	101	8	163	10	0.67	0.03	-10.1...	54	19	187	23	0.59	0.06
-7.1...	89	7	157	9	0.65	0.02	-12.9...	-1	34	238	35	0.44	0.06
-12.1...	124	6	156	7	0.63	0.02	-17.1...	-1	47	176	60	0.28	0.06
-21.0...	122	8	154	9	0.69	0.02							
-30.0...	166	11	115	19	0.60	0.04			NGC 4889	<PA>=81°			
-39.3...	188	20	173	25	0.65	0.05							
-47.2...	125	26	...	...	...	...	17.6...	-2	32	...	...	...	...
-53.3...	...	...	159	82	0.26	0.07	14.8...	...	...	382	92	1.26	0.32
		NGC 3379	PA=65				13.5...	-15	20	...	...	...	...
							10.4...	29	21	515	93	1.93	0.50
62.0...	...	...	107	71	0.18	0.04	8.1...	31	19	...	...	...	...
59.6...	31	34	...	...	...	...	7.6...	...	...	396	54	1.57	0.25
48.9...	46	23	145	36	0.33	0.05	6.2...	14	31	...	...	...	...
33.1...	33	19	178	30	0.43	0.05	4.8...	-1	39	463	58	1.68	0.28
22.8...	57	16	154	23	0.53	0.05	2.0...	49	19	266	30	1.04	0.09
15.9...	43	15	171	23	0.69	0.06	(0.0)[c]	-10	26	354	33	1.51	0.17
11.0...	30	12	181	18	0.78	0.06	-2.2...	-2	23	359	32	1.21	0.13
7.6[a]...	31	11	197	18	0.90	0.07	-4.2...	7	33	379	45	1.62	0.22
4.8[a]...	16	11	207	14	1.02	0.07	-6.1...	-16	27	302	42	1.22	0.17
2.0[a]...	11	12	231	15	0.99	0.07	-7.7...	-18	19	...	...	...	...
(0.0)[a,c]	-11	13	206	16	0.97	0.08	-10.2...	-15	19	277	48	0.89	0.14
-1.4[a]...	-22	11	211	15	0.99	0.08	-13.1...	0	29	...	...	...	...
-3.4[a]...	-37	12	216	15	1.00	0.08	-14.6...	...	...	466	151	1.46	0.59
-6.2[a]...	-58	14	224	20	0.95	0.09	-17.2...	-21	57	...	...	...	...
-9.0[a]...	-58	16	195	22	0.78	0.07							
-14.2...	-48	11	158	18	0.59	0.04			NGC 6909	PA=67°			
-24.3...	-49	20	155	31	0.45	0.05							
-33.9...	...	...	191	28	0.37	0.04	22.1...	29	12	110	22	0.54	0.04
-35.1...	-26	17	...	...	...	...	13.2...	16	9	127	13	0.54	0.02
-48.9...	-49	38	144	51	0.22	0.05	6.8...	22	8	121	11	0.57	0.02
-61.8...	-105	37	115	69	0.20	0.05	4.0...	22	12	117	18	0.56	0.04
							2.1...	23	14	100	20	0.58	0.04
		NGC 4839	<PA>=57°				-3.9...	-37	7	118	11	0.56	0.02
							-7.1...	-20	11	104	16	0.53	0.03
17.6...	1	36	230	40	0.62	0.09	-13.9...	-21	7	108	11	0.52	0.02
13.4...	-13	43	259	54	0.54	0.09	-25.6...	-59	18	118	32	0.49	0.05

[a] Corrected for beam bending; see § III.

[b] HGVS data alone—remainder average of HGVS and photographic data that has much lower γ.

[c] Bin centered on nucleus. Appropriate radius depends upon seeing, slit size, and surface brightness distribution. For uniform distribution, $r_{app} \sim 0''.7$, for HGVS data.

[d] Mean of dispersion from Sargent *et al.* 1977 and Tonry and Davis 1981.

APPENDIX B

Rotation and dispersion data for NGC 3379 have been collected and tabulated in Table 9. Velocities from Sargent *et al.* (1978) and Davies (1981) have been corrected by $V_{sys} = 905$ km s^{-1} and $V_{sys} = 893$ km s^{-1}, respectively. The sense of rotation for all three is that redshifted points lie SW of the nucleus (the minor axis is in PA 155°–335°). All three sets of data have been folded about the nucleus, by changing the sign of the corrected velocities for points NE of the nucleus.

Comparison of the error bars with the point-to-point scatter showed that all errors have been overestimated (see § V*c*). The factor is ~ 1.5 for the dispersion data from all three sources, ~ 1.5 for the velocity data from this paper, and ~ 1.8 for the velocity data from Sargent *et al.* and Davies. *The errors in Table 9 have been reduced by these factors.*

TABLE 9

NGC 3379: COLLECTED ROTATION AND DISPERSION DATA

log r (arcsec)	V (km s^{-1})	ΔV[a] (km s^{-1})	log σ (km s^{-1})	Δ(log σ)[a] (km s^{-1})	log r (arcsec)	V (km s^{-1})	ΔV[a] (km s^{-1})	log σ (km s^{-1})	Δ(log σ)[a] (km s^{-1})
PA 65°: This Paper					PA 49°: Davies 1981				
−0.15 ...	11	9	2.314	0.023	0.00 ...	−1	16	2.403	0.022
0.15 ...	22	7	2.324	0.021	0.57 ...	−9	8	2.301	0.020
0.30 ...	11	8	2.364	0.019	0.76 ...	−9	16	2.312	0.028
0.53 ...	37	8	2.334	0.020	0.92 ...	20	13	2.288	0.029
0.68 ...	16	7	2.316	0.019	1.12 ...	30	14	2.243	0.033
0.79 ...	58	9	2.350	0.026	1.25 ...	51	13	2.057	0.084
0.88 ...	31	7	2.294	0.027	1.35 ...	53	14	1.996	0.088
0.95 ...	58	11	2.290	0.033	1.50 ...	27	22	2.124	0.089
1.04 ...	30	8	2.258	0.029	1.61 ...	25	21	2.000	0.133
1.15 ...	48	7	2.199	0.033	1.81 ...	35	32	2.076	0.143
1.20 ...	43	10	2.233	0.039					
1.36 ...	57	11	2.188	0.043	PA 0°: Sargent *et al.* 1978				
1.39 ...	49	13	2.190	0.058					
1.52 ...	33	13	2.250	0.049	−0.16 ...	22	10	2.348	0.027
1.53 ...	...	...	2.281	0.043	0.23 ...	8	7	2.314	0.023
1.55 ...	26	11	...	...	0.49 ...	22	9	2.330	0.021
1.69 ...	49	25	2.158	0.115	0.61 ...	11	9	2.258	0.033
1.69 ...	46	15	2.161	0.072	0.81 ...	2	10	2.301	0.032
1.78 ...	31	23	...	...	0.87 ...	6	7	2.274	0.028
1.79 ...	105	25	2.061	0.174	1.14 ...	6	10	2.241	0.041
1.79 ...	...	...	2.029	0.192	1.15 ...	25	14	2.276	0.051

[a]Scaled; see Appendix B for correction factors.

REFERENCES

Bailey, M. E., and MacDonald, J., 1981, *M.N.R.A.S.*, **194**, 195.
Barbon, R., Benacchio, L., and Capaccioli, M. 1976, *Astr. Ap.*, **51**, 25.
Bertola, F., and Capaccioli, M. 1977, *Ap. J.*, **211**, 697.
Binney, J. 1978, *M.N.R.A.S.*, **183**, 501.
_____. 1980, *M.N.R.A.S.*, **190**, 421.
_____. 1981, in *The Structure and Evolution of Normal Galaxies*, ed. S. M. Fall and D. Lynden-Bell (Cambridge: Cambridge University Press), p. 55.
_____. 1982, *M.N.R.A.S.*, **200**, 951.
Binney, J., and de Vaucouleurs, G. 1981, *M.N.R.A.S.*, **194**, 679.
Boroson, T. 1981, *Ap. J. Suppl.*, **46**, 177.
Carter, D., Efstathiou, G., Ellis, R. S., Inglis, I., and Godwin, J. 1981, *M.N.R.A.S.*, **195**, 15P.
Davies, R. L. 1981, *M.N.R.A.S.*, **194**, 879.
_____. 1982, private communication.
Davies, R. L., Efstathiou, G., Fall, S. M., Illingworth G., and Schechter, P. L. 1983, *Ap. J.*, **266**, 39 (DEFIS).
Davies, R. L., and Illingworth, G. 1983, in preparation.
de Vaucouleurs, G. 1959, *Handbuch der Physik*, **53**, 311.
_____. 1975, in *Stars and Stellar Systems*, Vol. **9**, *Galaxies and the Universe*, ed. A. Sandage, M. Sandage, and J. Kristian (Chicago: University of Chicago Press), p. 557.
de Vaucouleurs, G., and Capaccioli, M. 1979, *Ap. J. Suppl.*, **40**, 699.
de Vaucouleurs, G., de Vaucouleurs, A. and Corwin, H. R. 1976, *Second Reference Catalogue of Bright Galaxies* (Austin: University of Texas Press) (RC2).
Dressler, A. 1979, *Ap. J.*, **231**, 659.
Dressler, A., and Sandage, A. 1983, *Ap. J.*, **265**, 664.
Efstathiou, G., Ellis, R. S., and Carter, D. 1980, *M.N.R.A.S.*, **193**, 931.
Faber, S. M. 1982, private communication.
Faber, S. M., Burstein, D., and Dressler, A. 1977, *A.J.*, **82**, 941.
Faber, S. M. and Jackson, R. E. 1976, *Ap. J.*, **204**, 668.
Freeman, K. C. 1970, *Ap. J.*, **160**, 811.
Fried, J., and Illingworth, G. 1983, in preparation.
Gregory, S. A. 1975, *Ap. J.*, **199**, 1.
Hodge, P. W., and Merchant, A. E. 1966, *Ap. J.*, **144**, 875.
Illingworth, G. 1977, *Ap. J. (Letters)*, **218**, L43.
_____. 1981, in *The Structure and Evolution of Normal Galaxies*, ed. S. M. Fall and D. Lynden-Bell (Cambridge: Cambridge, University Press), p. 27.
Illingworth, G., and Schechter, P. L. 1982, *Ap. J.*, **256**, 481.
Jarvis, B. J. 1982, Ph.D. thesis, Mount Stromlo Observatory, Australian National University, Canberra.
King, I. R. 1966, *A.J.*, **71**, 64.
_____. 1972, *Ap. J. Letters*, **174**, L123.
_____. 1978, *Ap. J.*, **222**, 1.
Kormendy, J. 1977, *Ap. J.*, **218**, 333.
_____. 1982, private communication.
Kormendy, J., and Illingworth, G. 1982, *Ap. J.*, **256**, 460 (KI).
Larson, R. B. 1974, *M.N.R.A.S.*, **166**, 585.
Malamuth, E., and Kirshner, R. P. 1981, *Ap. J.*, **251**, 508.
McElroy, D. 1981, Ph. D. thesis, Arizona State University.
Monet, D. G., Richstone, D. O., and Schechter, P. L. 1981, *Ap. J.*, **245**, 454.
Mould, J., Aaronson, M., and Huchra, J. 1980, *Ap. J.*, **238**, 458.
Nilson, P. 1973, *Uppsala Astr. Obs. Ann.*, Vol. **6** (UGC).
Oemler, A., Jr. 1976, *Ap. J.*, **209**, 693.
Sandage, A. 1972, *Ap. J.*, **176**, 21.
Sandage, A., Freeman, K. C., and Stokes, N. R. 1970, *Ap. J.*, **160**, 83.
Sandage, A., and Tammann, G. A. 1981, *A Revised Shapley-Ames Catalog of Bright Galaxies* (Washington: Carnegie Institute of Washington), Publication 635 (RSA).

Sargent, W. L. W., Schechter, P. L., Boksenberg, A., and Shortridge, K. 1977, *Ap. J.*, **212**, 326.
Sargent, W. L. W., Young, P. J., Boksenberg, A., Shortridge, K., Lynds, C. R., and Hartwick, F. D. A. 1978, *Ap. J.*, **221**, 731.
Schechter, P. L. 1980, *A.J.*, **85**, 801.
Schechter, P. L., and Gunn, J. E. 1979, *Ap. J.*, **229**, 472 (SG).
Terlevich, R., Davies, R. L., Faber, S. M., and Burstein, D. 1981, *M.N.R.A.S.*, **196**, 381.
Thuan, T. X., and Romanishin, W. 1981, *Ap. J.*, **248**, 439.
Tonry, J. L., and Davis, M. 1981, *Ap. J.*, **246**, 666.
Whitmore, B. C. 1980, *Ap. J.*, **242**, 53.
Whitmore, B. C., Kirshner, R. P., and Schechter, P. L. 1979, *Ap. J.*, **234**, 68.
Williams, T. B., and Schwarzschild, M. 1979, *Ap. J. Suppl.*, **41**, 209.
Wilson, C. P. 1975, *A.J.*, **80**, 175.

ROGER L. DAVIES and GARTH ILLINGWORTH: Kitt Peak National Observatory, P.O. Box 26732, Tucson, AZ 85726-6732